Pure Appl. Geophys. 178 (2021), 2419–2436

https://doi.org/10.1007/s00024-020-02604-y

Pure and Applied Geophysics

Performance of the International Monitoring System Seismic Network Based on Ambient Seismic Noise Measurements

Peter J. Gaebler[1] and Lars Ceranna[1]

Abstract—All nuclear explosions are banned by the Comprehensive Nuclear-Test-Ban Treaty. In the context of the treaty a verification regime was put into place to detect, locate, and characterize nuclear explosions at any time, by anyone and everywhere on the Earth. The International Monitoring System, which plays a key role in the verification regime, was set up by the Preparatory Commission of the Comprehensive Nuclear-Test-Ban Treaty Organization. Out of the several different monitoring techniques applied in the International Monitoring System the seismic waveform approach is the most effective and reliable technology for monitoring nuclear explosions underground. This study introduces a deterministic method of threshold monitoring that allows to asses a lower body wave magnitude limit of a potential seismic event in a certain geographical region, that can be detected by those seismic stations being part of the International Monitoring System network. The method is based on measurements of ambient seismic noise levels at the individual seismic stations along with global distance corrections terms for the body wave magnitude. The results suggest that an average global detection capability of approximately body wave magnitude 4.0 can be achieved using only stations from the primary seismic network of the International Monitoring System. The incorporation of seismic stations from the auxiliary seismic network leads to a slight improvement of the detection capability, while the use and analysis of wave arrivals from distances greater than 120° results in a significant improvement of the detection capability. Temporal variations in terms of hourly and monthly changes of the global detection capability can not be observed. Overall, comparisons between detection capability and manually retrieved body wave magnitudes from the Reviewed Event Bulletin suggest, that our method yields a more conservative estimation of the detection capability and that in reality detection thresholds might be even lower than estimated.

Keywords: International monitoring system, seismology, detection capability, ambient seismic noise, body wave magnitude correction curves.

1. Introduction

Scope of this study is to provide an estimate of the global detection capability in terms of a minimal observable body wave magnitude (m_b) of a seismic event based on measurements of ambient noise levels at the seismic stations of the International Monitoring System (IMS) in the year 2013. Spatial and temporal dependencies of the global detection capability, as well as dependencies on parameters such as station outage, source type, noise level and distance range of the investigated wave arrivals, are examined. First some general information about the Comprehensive Nuclear-Test-Ban Treaty (CTBT) and the IMS seismic network are introduced in Sect. 1.1, followed by a brief introduction on the discrimination of natural and explosive events, as well as the estimation of the yield of the potential nuclear event in Sect. 1.2. The introduction is concluded by an overview over previous investigations on threshold monitoring in Sect. 1.3. Section 2 introduces the seismic network of the IMS in more detail and provides information about the utilized data. The method of seismic threshold monitoring based on the evaluation of the seismic ambient noise levels is presented in Sect. 3. Results of the estimation process and dependencies of the detection capability are presented and discussed in Sect. 4. Section 5 presents a comparison between catalog magnitudes from the Reviewed Event Bulletin (REB) and theoretically computed minimum observable magnitudes. A conclusion and summary of the results is provided in Sect. 6.

Electronic supplementary material The online version of this article (https://doi.org/10.1007/s00024-020-02604-y) contains supplementary material, which is available to authorized users.

[1] Federal Insitute for Geosciences and Natural Resources, Stilleweg 2, 30655 Hannover, Germany. E-mail: peter.gaebler@bgr.de

1.1. The Comprehensive Nuclear-Test-Ban Treaty and the International Monitoring System

The CTBT is a multilateral treaty which bans all nuclear explosions on the Earth's surface, underground, underwater or in the atmosphere. It was adopted by the United Nations General Assembly in 1996, but still has not entered into force, as eight countries are still pending to ratify the treaty. To detect, locate and characterize nuclear explosions at any given time, by anyone and in all environments, a verification procedure was put into place by the CTBT organization (CTBTO 2020). This regime consists of the IMS, consultation and clarification elements, confidence building measures and an on-site inspection procedure, which can be conducted in the case of potential treaty violations. The IMS, when completely installed, will consist out of 321 globally distributed measurement stations and 16 additional laboratories for radionuclide measurements. In the context of the IMS four different techniques are applied: seismic, infrasound, hydroacoustic and radionuclide monitoring technologies. The first three methods are attributed to the waveform technologies. These methods are able to detect waveform signals from any kind of explosion that takes place on the Earth's surface, underground or carried out below water, respectively. A fourth method, the radionuclide monitoring technique, is complementary applied to the three waveform approaches and is able to detect radioactive substances emitted from nuclear explosions and is therefore able to provide the unambiguous evidence of the nuclear character of an event.

1.2. Seismic Discriminants and Magnitude-Yield-Relation

The International Data Center (IDC) of the Provisional Technical Secretariat in Vienna usually registers more than a hundred seismic events every single day. The majority of the recorded signals has a natural origin and is for example caused by earthquakes at subduction zones, volcanoes or other geodynamic active regions. According to the Gutenberg–Richter-law (Gutenberg and Richter 1954), more than 13000 earthquakes with m_b greater than 4.0 occur annually. A m_b value of 4.0 roughly corresponds to an energy release of 1 *kt* TNT-equivalent, the monitoring threshold requested by the CTBTO, for a coupled underground explosion. Only a small proportion of earthquakes detected by the IMS have their origin in non-natural events, for example quarry blasts, mining induced events or, very rarely, nuclear explosions. For purposes of monitoring nuclear explosions it is important to discriminate these events from other events not of interest for the CTBT. Furthermore, if a nuclear event has been identified, it is of special interest to obtain information about the yield of the explosion. Seismic discriminants are often based on properties of the seismic source in terms of location and dynamics. Latitude and longitude of the event help to distinguish between on- and offshore events, location in terms of depth is of special interest, as events with great hypocentral depths are associated to natural earthquakes only, and can therefore be dismissed from the beginning on. A further basis are properties of the source dynamics and the accompanying difference in content of short and long period seismic waves emitted by the source as well as the different pattern of energy release. This differences in source dynamic properties are for example expressed in different ratios of seismic magnitudes (Kebeasy et al. 1998), comparisons of different wave type amplitude ratios (Richards and Kim 2007), the analysis of the (cross)-spectral ratios (Hartse et al. 1997) or in investigations of the moment tensor components (Cesca et al. 2017; Han et al. 2017; Liu et al. 2018; Gaebler et al. 2019). Once an event has been identified as a nuclear explosion, the determination of the strength of the explosions is of great interest. Explosions are usually assessed in yield equivalent to *kt* TNT, which is typically derived from m_b. It is in general not possible to state one single relation between magnitude and yield, as this relation depends on many factors (National Research Council 2012), such as the geological setting at source site, the efficiency of wave propagation from source to receiver, depth of the explosion and the coupling of the source to the subsurface. Formulas of the type $m_b = A + B\log(Y)$ are in general used to relate magnitude and yield. Here Y is yield in *kt* TNT-equivalent and A and B are constants depending on

the aforementioned factors. For m_b-Y relations the reader is for example referred to Murphy (1981) or Ringdal et al. (1992).

1.3. Previous Studies on Seismic Threshold Monitoring

The evaluation of the detection capability of seismic networks (for example the IMS network) is typically based on the assumptions of statistical models of the ambient seismic background noise at the stations as well as of the distribution of the seismic signals. The detection capability of the system is assessed as a function depending on the number of phase detections that are necessary for the dependable positing finding of the event (Kværna and Ringdal 1999). These models result in maps depicting the local, regional or global detection capability of the network. For studies using this approach see for example Harjes (1984) or Ringdal and Kværna (1992). Continuous threshold monitoring is a complementary method that can address these issues and is a useful supplement to the event detection analysis . This method is able to continuously monitor a specific area and therefore provide continuous assessments of the upper magnitude limit of a possible event that might have occurred in the region of interest (Ringdal and Kværna 1992). Ringdal and Kværna (1992) for example applied site specific threshold monitoring, a method which focuses a seismic array on a target region to continuously provide threshold monitoring for that site. For a further example of continuous threshold monitoring see for example Ringdal and Kværna (1989). The study presented here provides time dependent (hourly and monthly) global maps of the detection capability of the IMS seismic network for the year 2013. For a description of the applied method see Sect. 3.

2. Seismic Stations and Ambient Seismic Noise Data

In this study ambient seismic background noise data from the IMS seismic network is used. The IMS seismic network can be considered as the backbone technology for monitoring underground nuclear explosions. The seismic approach relies on waves propagating through the Earth's interior, which can be registered and recorded at the seismic stations of the IMS network. Seismic waves are mostly generated by natural earthquakes, but may also find its source in natural events such as meteorites or landslides as well in manifold anthropogenic sources. The seismic signals travel with speeds of up to several kilometers per second and can therefore be registered at the seismic stations only seconds to minutes after the origin time of the seismic event. The seismic IMS network, when fully deployed, will consist out of 170 seismic stations, assigned to two different kinds of networks. The first network is the primary seismic (PS) network, which, when completed, will contain 50 seismic stations with continuous data transmission in near real time to the IDC. The second type of seismic network, the auxiliary seismic (AS) network, will consist, as soon as fully deployed, out of 120 stations. In contrast to the PS stations, data from the AS stations is only transmitted to the IDC upon request. In addition to the PS and AS stations, five stations from the hydroacoustic (HA) network are equipped with standard seismic instruments and can consequently be used in the global detection capability estimation process.

In general two different types of stations can be differentiated: Seismic array stations and three-component (3C) stations. Array stations consist out of a multitude of individual sensors arranged in an optimized geometric pattern, usually covering areas from a few to hundreds of square kilometers. The number of individual sensors ranges from only few up to more than 40 sensors. Seismic arrays allow for an improvement of the signal to noise ratio (SNR) and provide information about direction and speed of the incoming wave-field (see, e.g., Rost and Thomas (2002)). 3C stations only consist out of one single instrument that measures the components of translational motion of the seismic wave-field in three orthogonal directions. In comparison to seismic arrays, the single station approach results in a lower SNR and therefore has bigger uncertainties in the evaluation of the measured seismic signals. The global distribution of the seismic IMS stations is illustrated in Fig. 1. For more detailed information the reader is for example referred to Pilger et al. (2017) or CTBTO (2020).

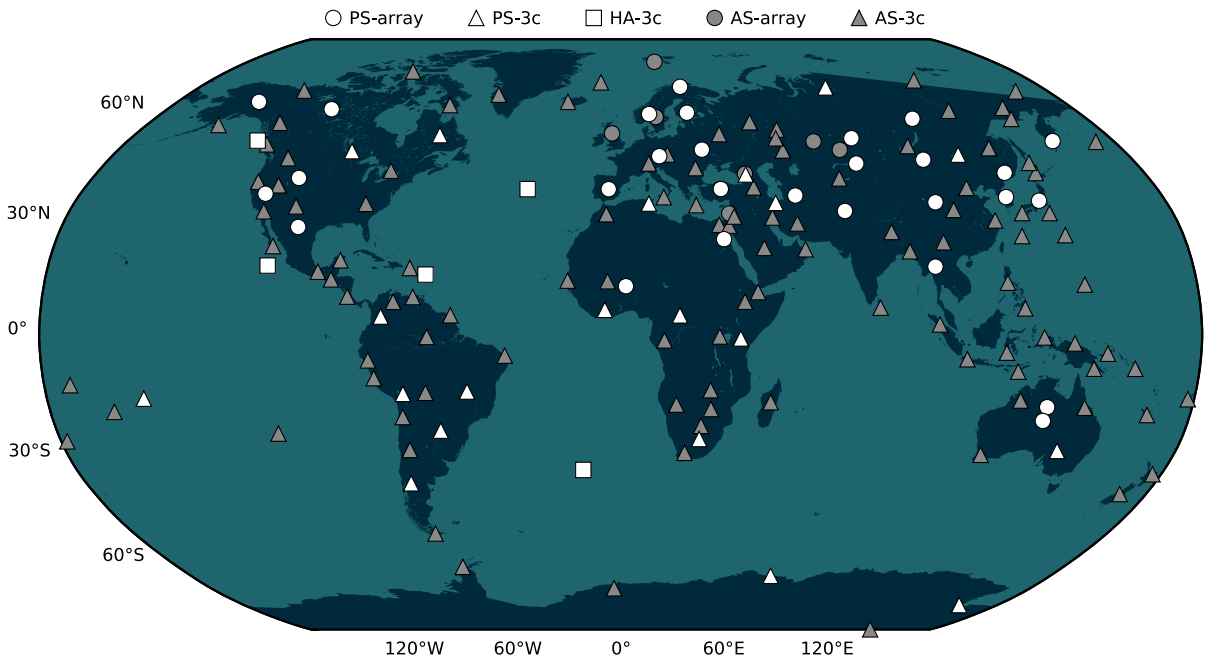

Figure 1
Seismic network of the IMS. World map showing locations of the PS and AS stations, as well the HA stations. PS and HA stations are marked in white, AS stations are illustrated in grey color. Circles represent array stations, triangles indicate 3C seismic stations, squares indicate 3C HA stations. The map shows stations irrespective of the station status (certified, planned, under construction, installed but not yet certified)

In this study all stations shown in Fig. 1 are incorporated in the global detection capability estimation process, irrespective of the current operational station status (certified, planned, under construction, installed but not yet certified). If no ambient seismic noise data was available for a certain station, an average noise level value, calculated from the closest stations in setting (e.g. island stations are compared to island stations), was assumed. Data was available throughout the year 2013. For each month hourly average noise levels were computed by taking the average noise levels from all days of the respective month. This consequently results in 24 noise level measurements for each month for each individual station. Noise level data was available in the form of power spectral density (PSD) functions. For information on the PSD functions see Brown et al. (2014). An example of the PSD functions for three different stations is given in Fig. 2.

Figure 2 illustrates the PSD average, low and high noise level functions for the IMS stations PS19 in Germany, AS035 in Antarctica and AS024 on the Cook Islands in January 2013, 00:00–01:00 (UTC). A clear difference in the PSD noise levels is observable between the stations in the frequency band 0.8–2.2 Hz, which is of main interest for the estimations of the global detection capability. Stations PS19 and AS035 show a noise level of around −155 dB in the investigated frequency band, while station AS024 has a noise level of approximately −130 dB. This large difference emerges from the different locations of the stations. While stations PS19 and AS035 are located in remote and very calm regions, station AS024 is placed in a very noisy environment on an exposed island.

3. *Method for Estimating the Global Detection Capability*

Here the method of seismic threshold monitoring is introduced for assessing a lower magnitude limit of a potential seismic event in a certain given geographical region. The global detection capability of

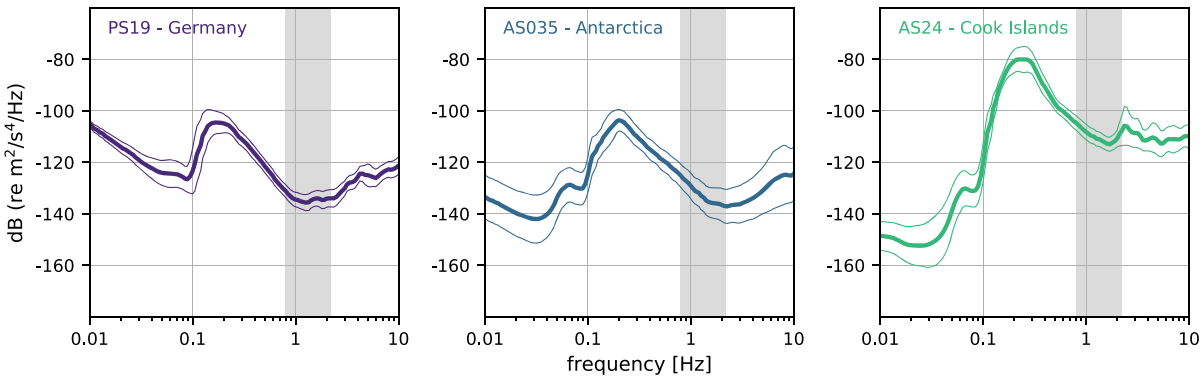

Figure 2
PSD functions for three different IMS seismic stations for the time 00:00 to 01:00 (UTC) in January 2013. Figure shows examplary average (thick line), low and high (thin lines) noise levels for the PS array station PS19 in Germany, as well as for the two AS 3C stations AS035 in Antarctica and AS024 on the Cook Islands. Grey shaded area depicts the frequency range from 0.8 to 2.2 Hz, which is used in the detection capability estimation process

the IMS seismic network is estimated using a technique based on the ambient seismic background noise measured at the individual stations (compare Fig. 2) of the IMS network as well as on global distance correction terms for m_b, which are calculated using the seismic reflectivity method. The calculated correction curves are consequently used to determine the minimum magnitude of a seismic event required at a certain geographic location to cause a signal of an amplitude that can be distinguished from the background ambient noise at the individual stations. The first step involves the estimation of detection threshold values D at the individual stations of the IMS seismic network. D is a measure for the minimum amplitude of a seismic signal caused from an event recorded at a seismic station, that can be discriminated from the seismic background noise. Station specific average, low and high seismic background noise levels are extracted from the PSD functions of the different IMS stations in a frequency range from 0.8–2.2 Hz, the typical frequency range for teleseismic P- and PKP-waves. From the *dB* values in the PSD functions absolute ground velocity values V in m/s for the individual stations are calculated. To discriminate the arrival of a seismic signal from the background noise, the signal has to exceed the noise level V by a certain amount. For stations with array configurations the threshold value D is corrected by a factor of $\sqrt{N}$, where N is the number of sensors in the seismic array. This reduction of the threshold value is possible due to different special properties of seismic arrays, such as beamforming [see, e.g., Rost andThomas (2002); Coyne et al. (2012)]. The total threshold D value is consequently calculated as

$$D = \frac{SV}{\sqrt{N}}, \tag{1}$$

where S is the required SNR, V is the measured ambient noise levels and N is the number of sensors of the individual IMS stations. The next step requires the calculation of global m_b correction terms over the entire distance range from 0° to 180°. The computations are based on empirical global depth-distance correction terms based on seismic moments given by Rezapour (2003). New global correction terms for m_b in the distance range between 20° and 100° using the values of the scalar moment M_0 in the Harvard Centroid Moment Tensor catalog (Dziewonski and Anderson 1981; Ekström et al. 2012) to calibrate P-wave amplitude-distance curves were determined by Rezapour (2003). The additional inclusion of correction terms for the distances 0–20 degrees and 120–180 degrees, and therefore to be able to include seismic phases such as Pg, Pn and PKP, is achieved by using calculations based on the seismic reflectivity method. Values given by (Rezapour 2003) are used for scaling the results from the reflectivity method. Reflectivity modeling was first introduced by (Thomson 1950). The propagation of seismic waves

is simulated in the frequency-wave number domain in a cylindrical coordinate system. This choice of coordinate system allows the reduction of the wave equation to one dimension, backtransform of the results into the frequency time domain is possible using the Fourier transform. Reflectivity modeling incoporates the decomposition of seismic waves into up- and down going waves in the layers, the waves can be decoupled into P-, SV- and SH-waves (Kennett 1983). The method includes reflections, transmissions and conversions between the different wave modes and allows to include different conditions, for example the free surface condition. Main advantages of the reflectivity method are its ability to model nearly all kinds of seismic waves, including surface waves (Haskell 1953) in elastic and anelastic media with high numerical stability while keeping computational costs low. See for example Fuchs and Müller (1971) and Müller (1985) for studies applying the reflectivity method.

In this study we apply the reflectivity method described and coded by Müller (1985). We use a standard AK135 velocity model (Kennett et al. 1995) and attenuation values from the Preliminary Reference Earth Model (Dziewonski and Anderson 1981) for a center frequency of 1 Hz. Synthetic seismograms are recorded at receivers placed every 50 km in the distance range from 0° to 55°. For distances greater than 55° receiver distance is set to 100 km. To average P-phase amplitudes at the surface synthetic seismogramms for 20 arbitrary double couple sources have been computed. To simulate a shallow source, source depth in all cases is set to 2 km. Dominant source frequency is set to 1 Hz. A combination of results from the reflectivity simulations and the findings from Rezapour (2003) yields distance dependent m_b correction terms covering the entire distance range. The correction terms calculated for a near surface averaged double couple source, as well as for a near surface explosive source, are depicted in Fig. 3.

The calculated distance dependent m_b correction terms show noticeable differences to the corrections factors provided in a study by Murphy and Barker (2003) in the distance range of around 145°. In this distance range mainly refracted core phases (PKPab, PKPac and PKPdf) can be observed (see also Sect. 4.3). The observation that our correction terms in this distance range are significantely lower than the terms provided by Murphy and Barker (2003) can be attributed to the fact that our correction terms reflect a theoretical minimum detectable mb-values for PKP-phases recorded at stations with a realistic noise level. In contrast to this, Murphy and Barker (2003), as well as Kværna and Ringdal (2013), considered minimum detectable m_b values based on REB events. Since most automatic seismic event lists (SEL) at the IDC are build on at least three defining stations covering the full distance range, it is most likely that at least one defining station is in a teleseismic distance range between 20° and 90°. Consequently, the minimum m_b values of an SEL event lie between 3.4 and 4.0.

A global grid with dimensions of 0.5° in latitudinal and longitudinal direction is specified. This results in a total 259200 grid cells. For each pair of grid cells and stations a minimum detectable magnitude can now consequently be assigned using following equation for the distance dependent m_b curves (Gutenberg and Richter 1956):

$$m_b = \log\left(\frac{D}{T}\right) + C. \tag{2}$$

Here T is the dominant period of the investigated seismic signal and C represents the distance dependent correction terms for m_b (compare Fig. 3). This step results in n minimum observable magnitudes for each grid cell, where n is the number of stations used in the estimation process. To detect and estimate the magnitude at any given point a minimum number of stations is required to be able to record and distinguish the signal from the disturbing background noise level. In this study a minimum of three stations is required. Subsequently the minimum magnitude observable at a certain grid cell, is the third lowest magnitude from the n magnitudes calculated from the n grid cell – station pairs. Three different models for the global detection capability of the IMS seismic stations are consequently obtained: an average, a low and a high noise model. The results of the estimation process as well as the dependencies of the global detection capability on certain parameters are presented and discussed in Sect. 4.

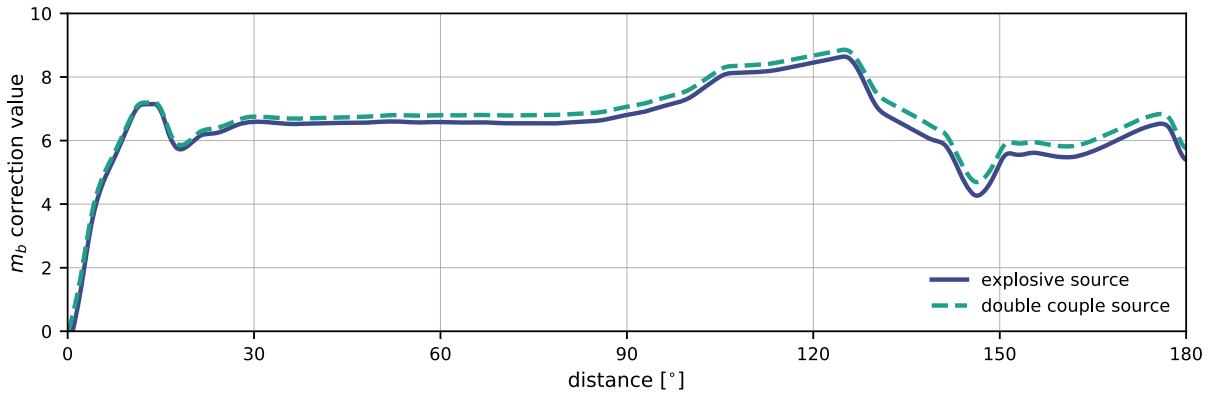

Figure 3
Distance dependent m_b correction curves. Green dashed line indicates correction terms for a shallow DC source, solid blue line represents the correction curve for a near surface explosive source. Throughout the entire distance range explosion correction terms are smaller than double couple correction terms, this is explained by reflections of seismic energy at the surface in the explosive source process. Correction curves are based on results from Rezapour (2003) and on wave propagation simulations using the seismic reflectivity method

4. Detection Capability and Dependencies

This section features the results of the detection capability estimation of the seismic IMS network. The spatial dependency as well as the influence of the choice of network on the detection capability is presented in Sect. 4.1, the temporal properties of the threshold monitoring are analyzed in Sect. 4.2. In Sect. 4.3 the use of wave arrivals from different distance ranges is evaluated, while Sect. 4.4 investigates further dependencies of the detection capability such as assumed source type, number of operational stations and choice of noise level.

4.1. Spatial Dependency and Influence of Choice of Network

The global detection capability of the IMS seismic network shows a strong spatial dependency and is significantly influenced by the choice of the utilized networks (PS, AS, HA). This dependencies are exemplary illustrated for the time span 12:00–13:00 UTC in January 2013 in Fig. 4.

Figure 4a illustrates the global detection capability using only PS and HA stations. The minimum observable magnitude estimations are based on the average noise level for the time 12:00–13:00 (UTC) in January 2013. Distance ranges of seismic wave arrivals that are included in the estimation process are 0°– 120°, this includes wave traveling on local to regional distances such as guided P- and S-waves in the mantle, as well as it includes the arrival of the direct P-wave in the distance range from 20° to 90°. Waves of distances greater 120° are excluded, such as arrivals from PKP-waves, waves that travel through the Earth's outer core. A minimum SNR of three is required for the signal to be able to be observed, the minimum number of detections necessary for the identification of an event is set to three. A shallow DC source is assumed for the calculation of the distance dependent m_b correction curves (compare Fig. 3). We furthermore use the average noise levels of the stations (compare Fig. 2). In total an average global detection threshold of $m_b \sim 4.0$ is achieved. Due to the heterogeneous station distribution, a significantly higher number of stations is located on the northern hemisphere, a clear difference in the detection capability is observable between northern and southern hemisphere. On the northern hemisphere an average value of $m_b = 3.9$ can be detected, with values being as low as 3.6 to 3.8 in specific regions such as North America or Europe. In contrast the average value for the detection capability on the southern hemisphere has an average value of $m_b = 4.2$, with magnitudes reaching values of up to 4.6 in specific regions (South Atlantic, Antarctica). In contrast to the strong latitudinal dependency, no significant longitudinal dependency can be observed.

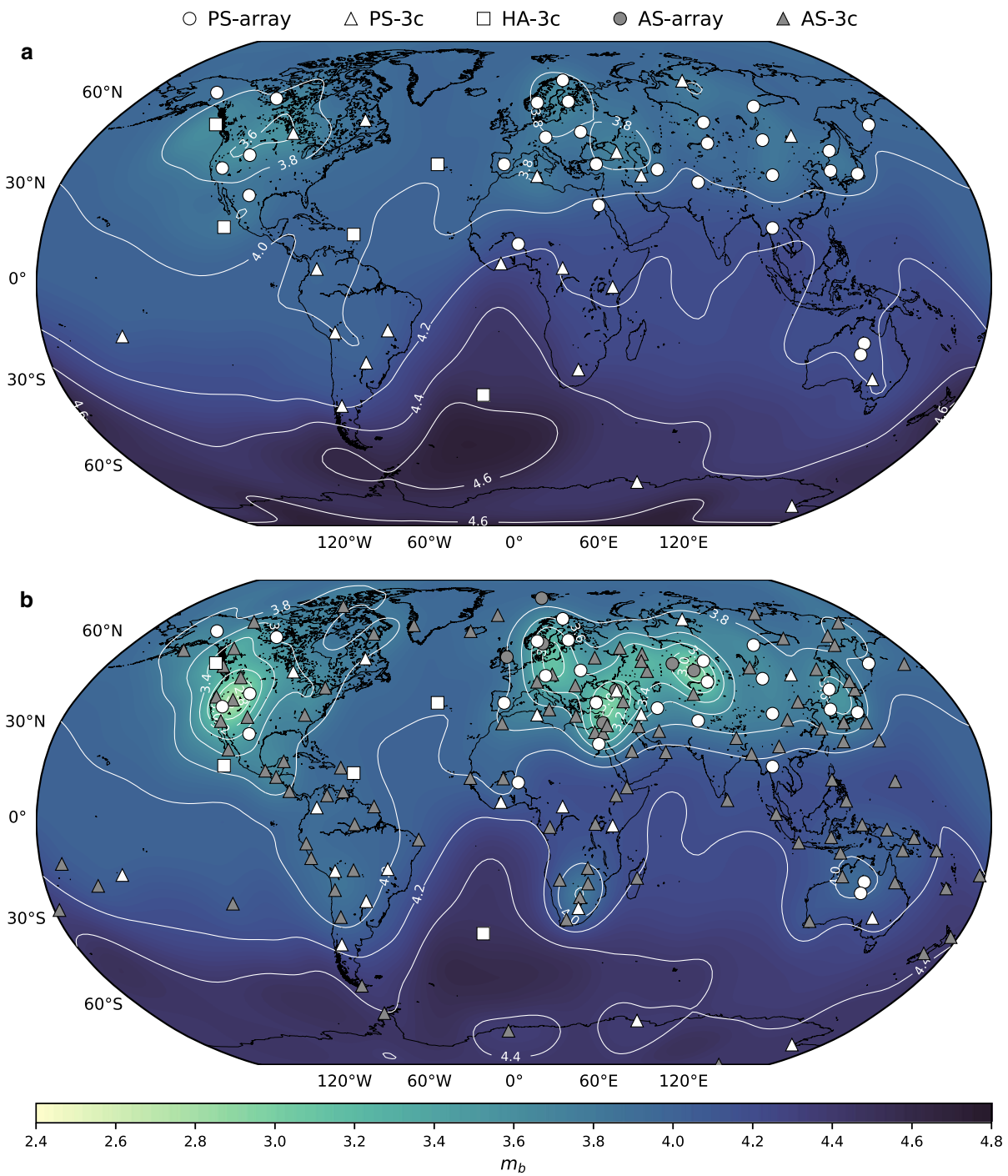

Our estimations of the detection threshold are similar with findings from for example Harjes (1984). Harjes (1984) used a network of 50 globally distributed stations to estimate a magnitude threshold for teleseismic detections in the range between $4.0 < m_b < 4.5$ for the northern part of the globe and $4.5 < m_b < 4.9$ for the southern hemisphere. For specific regions (for example Scandinavia or North America) the detection capability reaches values from as low as 3.4, other regions show significantly

◀Figure 4
Detection capability of the IMS seismic network. World map depicting the minimum magnitude detection capability based on average noise measurements of the IMS seismic network in January 2013 (12:00–13:00 UTC). The SNR required for the detection of a signal is set to three, the minimum number of detections necessary for the identification of an event is three. Seismic phases from the distance range 0°–120° are used in the estimation process. Background color indicates minimum detectable magnitude. **a** Only stations from the PS network and from the HA network are used. PS arrays are depicted with white dots, PS 3C stations are represented as white triangles. HA stations are given as white squares. **b** Same as top part of the figure, but additionally to the PS and HA stations, data from the AS network is used in the estimation process of the detection capability. AS array stations are shown as grey dots, AS 3C stations are given as grey triangles

higher values for the magnitude threshold (Antarctica, New Zealand, Southern Atlantic region). This also coincides with our results. Our findings are also supported by results from Ringdal (1986), who estimated values of $3.9 < m_b < 4.5$ for the northern hemisphere and values of $4.2 < m_b < 4.8$ for the southern hemisphere. A study by Kværna and Ringdal (2013) estimated a network detection capability of the PS network of $m_b = 3.7$ or better across the entire globe and m_b values of as low as 3.0 in selected areas. These areas inlcude parts of Europe, Central Asia and North America. The authors found the detection threshold to be higher on the southern hemisphere, especially in oceanic regions and Antarctica. These areas of higher or lower detection threshold are in good agreement with the findings of this study. The in general lower detection threshold values for the entire globe in the study by Kværna and Ringdal (2013) compared to results from this study can by explained by two reasons. First, the noise levels in this study are obtained from instrument-corrected acceleration spectra averaged in a frequency band from 0.8–2.2 Hz. In reality, the detection of seismic signals is usually performed on raw waveform velocity data. As a consequence, for many seismic stations located on Eurasian, North American and Australian shield areas, teleseismic signals from events near the detection limits are often clearer observed at higher frequencies (e.g. 2–4 Hz). For local and regional events, frequencies may even be higher. Therefore, the noise levels in this study obtained from the acceleration spectra averaged over the frequency range 0.8–2.2 Hz might be overestimated. Second, Kværna and Ringdal (2013) subtract a constant value of $m_b = 0.184$ from the calculated detection capability estimates to make the results compatible with previously published estimates that are based on m_b amplitude-distance curves given in a study by Veith and Clawson (1972). An improvement of the detection threshold can be achieved by including stations from the AS network. This incorporation leads to a global improvement of around $m_b = 0.1$ and is illustrated in Fig. 4b. In some regions, where only few PS and HA stations are present and where the inclusion of the AS-stations leads to a densification of station coverage a more significant improvement can be observed. These areas for example include the region of the western Unites States, Eastern Europe, the Middle East and the Kazakhstan region. Minimum observable magnitudes show values of as low as m_b =3.2 for these specific regions. See also electronic supplementary material for a difference plot between Fig. 4a, b. Figure 5 gives an overview over the latitudinal and longitudinal spatial dependency of the detection capability for the two scenarios presented in Fig. 4.

Figure 5 illustrates average m_b values for a given latitude or longitude and clearly underlines the strong latitudinal dependency as well as the improvement of the detection capability resulting from the inclusion of the AS stations in the estimation process.

4.2. *Temporal Dependency of the Global Detection Capability*

This subsection contains information about the temporal dependency of the detection capability in the year 2013 in terms of hourly and monthly variations. Figure 4 only shows a snapshot of the global detection capability of the network for one particular time frame, but all times investigated (24 time frames for each of the 12 months) show a very similar pattern and size of the minimum detectable magnitude. As an example Fig. 6 shows the global detection capability of the network for the time 12:00–13:00 (UTC) in July 2013 under the same assumptions as made in Fig. 4.

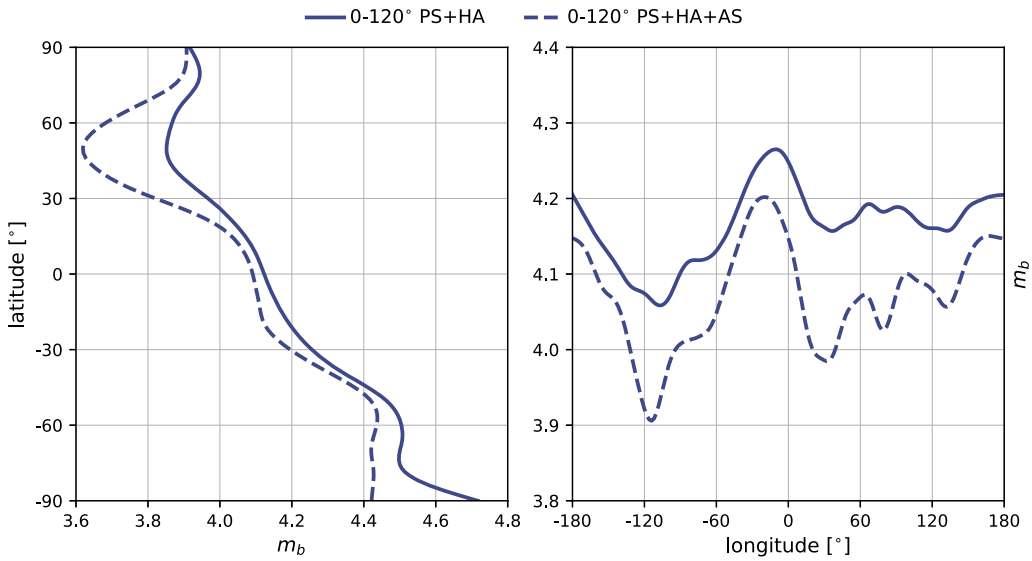

Figure 5
Spatial dependency of the IMS network detection capability. (left) Latitudinal and longitudinal dependency of the IMS network detection capability for the two scenarios presented in Fig. 4. Curves are average m_b values for a given latitude or longitude. Solid blue lines represent detection capabilities using only PS and HA stations and wave arrivals in the distance range 0°–120°, dashed blue lines indicate detection capability estimate with the additional use of stations from the AS network

When comparing the time frames January and June 2013, no significant differences can be spotted between the two time frames, average minimum detectable magnitudes are similar for northern and southern hemisphere. Furthermore, areas with significantly lower or higher magnitude thresholds (for example Scandinavia, Antarctica) are identical in both presented time frames. Our data set allows not only to investigate the monthly variations, but also offers the opportunity to look at hourly variations during the day. This variations are exemplary shown in terms of latitudinal variations in Fig. 7 for January and June 2013, typical months for northern hemispheric early winter and early summer.

As already mentioned no significant differences can be observed between the two months of the year 2013. Furthermore, no differences during the 24 h of the day can be observed. Observable minimum magnitudes are similar during the cause of the day for all twelve investigated months and no influence of the day-night cycle can be observed. We conclude that hourly or seasonal temporal variations do not significantly influence the global detection capability of the IMS seismic network.

4.3. Inclusion of PKP-phase arrivals

In the previous estimations of the detection capability in this study only wave arrivals in the distance range from 0° to 120° were included. The inclusion of wave arrivals from distances greater than 120° leads to a significant improvement of the global detection capability of the IMS seismic network. This is mainly attributed to the fact, that in the distance window of around 145° refracted core phases are able to provide very good detection possibilities, sometimes even better than the direct P-waves (Harjes 1984). At around 145° three types of core refracted P-phases (PKPdf, PKPbc and PKPab), which have traveled along different paths through the Earth's inner and outer core, arrive at nearly the same time at theseismic receiver (Bormannetal 2009). Therefore their energies may superimpose and yield an arrival with a very high amplitude, consequently resulting in smaller m_b correction terms (compare Fig. 3) and therefore help to lower detection thresholds (Qamar 1973). For further information on seismic PKP phases we also refer the reader to the IASPEI standard phase list (ISC 2020). The inclusion of these wave arrivals is illustrated in Fig. 8.

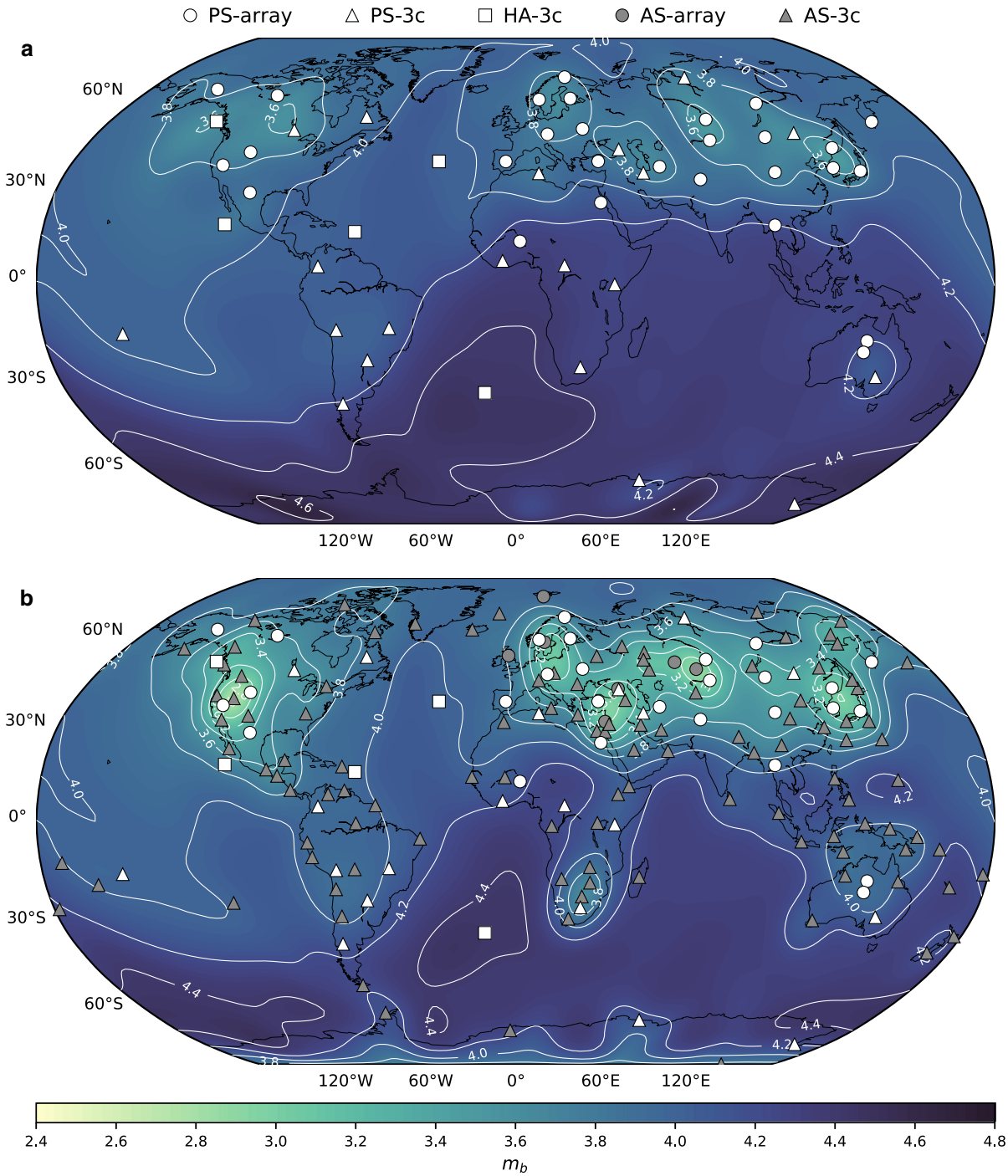

Figure 6
Detection capability of the IMS seismic network. Same as Fig. 4, but for the time frame June 2013 (12:00–13:00 UTC)

The inclusion of phases from distances greater than 120° leads to a strong decrease of the detection threshold. Using only PS and HA stations (Fig. 8a) a global decrease of the average threshold value of

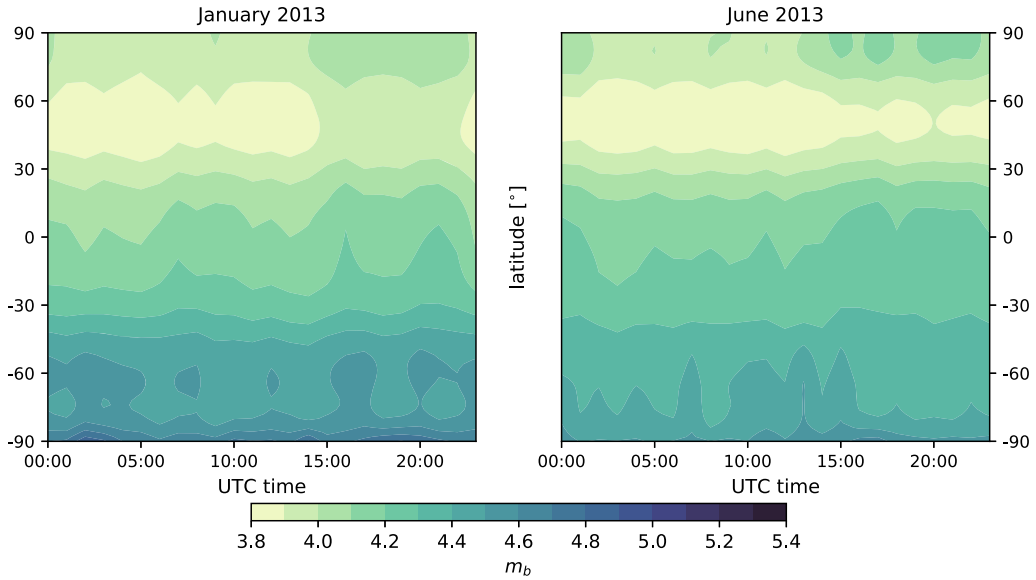

Figure 7
Temporal dependency of the detection capability of the IMS network. Figure shows latitudinal dependency of the detection capability of the IMS network over 24 h for the months January (left) and June (right) 2013. Background colors indicate minimum detectable magnitudes

around 0.6 units m_b can be achieved, with the largest decrease (1.0) for the southern hemisphere. For the northern hemisphere an improvement of around 0.2 units m_b can be observed. This can easily be explained by the heterogeneous station distribution, as stations on the northern hemisphere are now especially sensitive to events occurring on the southern hemisphere and vice verse when including the PKP-branches. However, we note that these large increases in detection capability using PKP-phases are based on idealized synthetic simulations and might therefore not reflect the actual detection capability of the IMS network, especially in the light of a limited localization capability using PKP-arrivals, only. The inclusion of AS stations leads to an overall improvement of around 0.2 for the detection capability and is illustrated in Fig. 8b. For better comparison the spatial dependency of the four scenarios shown in Figs. 4 and 8 is summarized in Fig. 9.

Difference plots between the scenarios given in Figs. 8a, b, Figs. 4a and 8a, as well as Figs. 4b and 8b, are presented in the electronic supplementary material to this manuscript.

4.4. *Dependency on Source Type, Noise Level and Number of Operational Stations*

As a final aspect the influence of source type, noise level and number of operational stations on the detection capability of the IMS network is examined. These three dependencies are jointly illustrated in Fig. 10.

Figure 10 shows the average global detection threshold for a DC source (left) and an explosive source (right) for a different number of operational PS stations. Furthermore global detections capabilities are shown for different assumptions of noise levels at the stations: average, low and high (compare Fig. 2). Station outage was simulated by randomly removing a certain percentage of PS stations from the estimation process. To obtain multiple realizations of station distribution, 100 estimations with different randomly removed stations were calculated for each station outage percentage. Noise levels from the time frame January 2013 (10:00–11:00 UTC) were used, wave arrivals from the distance range 0°–120° were utilized. A difference of around 0.3 units m_b is observed between average and high amplitude noise levels, as well as between the average and low amplitude noise levels. This numbers hold true for all

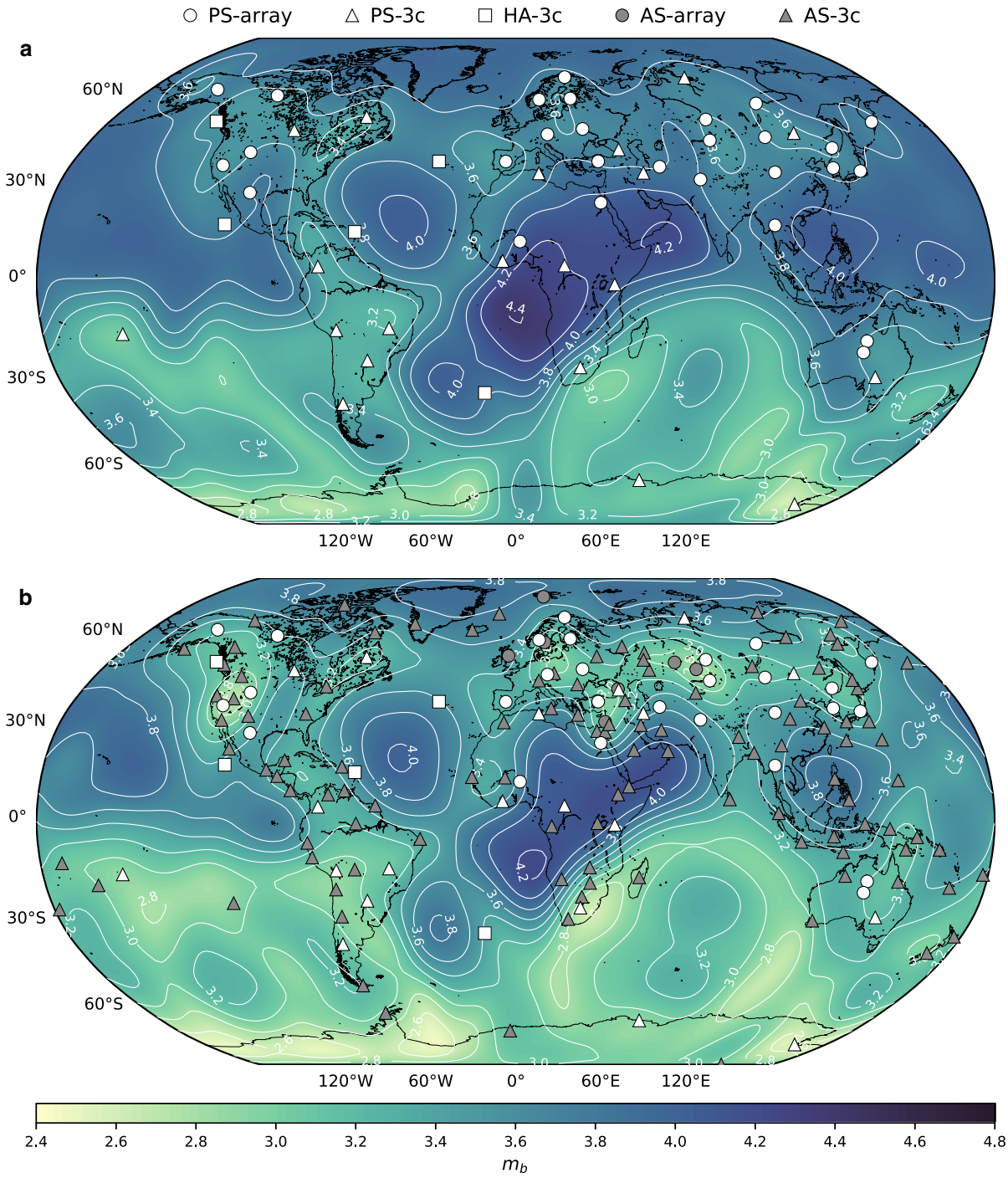

Figure 8
Detection capability of the IMS seismic network. Same as Fig. 4, but for the entire distance range (0°–180°) of included wave arrivals

numbers of operational stations as well as for both investigated source types. The difference in average global detection capability between DC source and explosive source is around 0.2 units m_b for all number

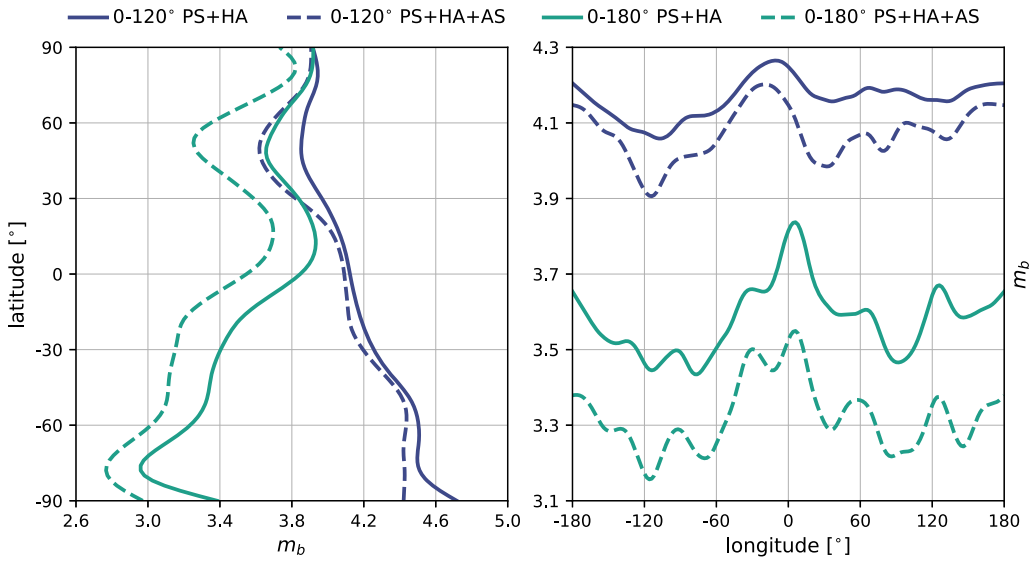

Figure 9
Spatial dependency of the IMS network detection capability. Same as Fig. 5, but also showing the latitudinal and longitudinal dependency for the scenarios presented in Fig. 8 (green lines)

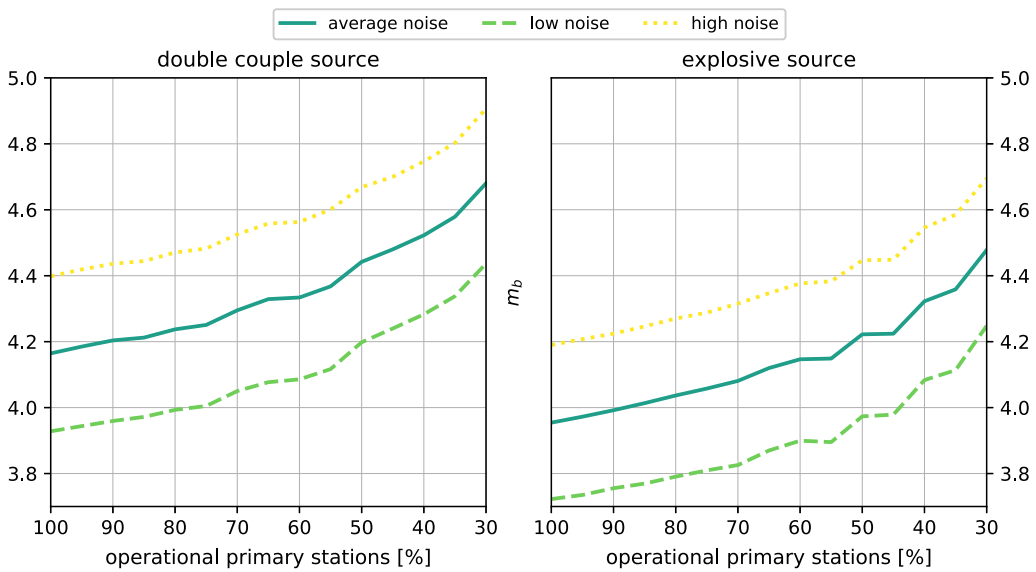

Figure 10
Influence of station outage, expressed by outage of PS-stations in percent, and different source types on the global detection capacility. Shown is the average global detection capability of the IMS network for an average (dark blue), a low (yellow) and a high (light blue) noise level for different numbers of operational PS-stations. Time frame for the estimations is January 2013 (12:00–13:00 UTC). (left) Global detection capability for a shallow double couple source. (right) Global detection capability for a shallow, purely compressional source

of operational stations and for all investigated noise levels. This number can be calculated from the two different m_b correction curves for a DC and explosive source presented in Fig. 3. At the current status, 44 out of the 50 (88 %) planned stations of the PS network are certified and operational. Our

simulations suggest an increase of below 0.05 units m_b for this percentage of operational PS stations when compared to a fully deployed and operational network. Assuming a station outage of 50 % the magnitude threshold on average increases around 0.2 units m_b, with a further increase of around 0.2 when considering only 30 % operational PS stations.

5. Comparison with Detections from the Reviewed Event Bulletin

The REB from the CTBTO has been reviewed by a human analyst and contains a list of events recorded at the seismic, hydroacoustic and infrasound stations of the IMS network. It includes information about source time, location and magnitude of the event, as well as attributes that describe every signal that is associated to the event. In Fig. 11, distance dependent minimum observable magnitudes estimated using the method described in Sect. 3 are compared to event magnitudes from the REB. Here we show comparisons for three stations of the PS network: Station PS03 (ASAR, Australia), station PS19 (GERES, Germany) and station PS06 (LPAZ, Bolivia). Event magnitudes, which have at least one phase association to the PS station are shown, distances given in the figure are epicentral distances from the event to the PS station.

In general a good agreement, especially in the distance range from 0° to 120° can be observed between magnitudes obtained from the REB and magnitudes calculated using our theoretical ambient noise based model at the three stations shown in Fig. 11. However some issues and discrepancies between the magnitudes in certain distance ranges have to be addressed and discussed. Deviations between the REB magnitudes and the predicted magnitudes in the distance range 0°–20° can be explained by the mean interstation distance of around 15° when considering all PS stations. In reality, with only a lesser number of PS-stations being operational, the mean interstation distance even increases and amplifies the discrepancies in the close range. Variations in the range 100°–130° can be caused by arrivals from PP-phases at the stations as well as possible conversions from S- to P-energy. The largest deviations appear in the distance range 140°–155°. Our theoretical, noise based model predicts m_b values down to 2.1. This is not observed in the comparisons of theoretical curves and REB events, as the magnitudes of the REB events are defined using P-wave phases at stations in the distance range 20°– 90°. This is also visible in the fact, that the REB magnitudes in the distance range 20°–90° are similar to the REB magnitudes in the distance range 140°–155°. Note that the theoretical prediction of an lower limit magnitude results in a very conservative detection capability estimation.

6. Conclusions

We introduce a method based on the measurements of ambient seismic noise levels to estimate the global detection capability of the IMS seismic network in the year 2013. Our results suggest a global average m_b threshold of around 4.0 using only seismic stations of the PS- and HA-network and solely including wave arrivals from the distance range 0°–120°. A clear latitudinal dependency can be observed with an average value of 3.9 on the northern hemisphere and an average threshold value of 4.2 units m_b on the southern hemisphere. No dependency on the longitudinal position of the event on the detection capability is suggested. The inclusion of stations from the AS-network in the estimation process leads to an average improvement of the monitoring threshold of 0.1 units m_b. Taking into account wave arrivals from distance ranges greater than 120° (mainly refracted core phases) strongly lowers the detection threshold value to a global average of around 3.6, with values on the northern hemisphere being as low as 3.8 units, on the southern hemisphere values are even as low as 3.3 units m_b. We furthermore are not able to observe any form of temporal variation in terms of hourly or seasonal variations of the noise field. The assumption of an explosion source lowers threshold values by 0.2 units m_b. The current status of the network (44 operational PS stations) only leads to an increase of less than 0.05 units m_b, when compared to the detection capability of a fully operational network (50 PS stations). Comparisons to REB magnitudes suggest, that our estimations only yield a

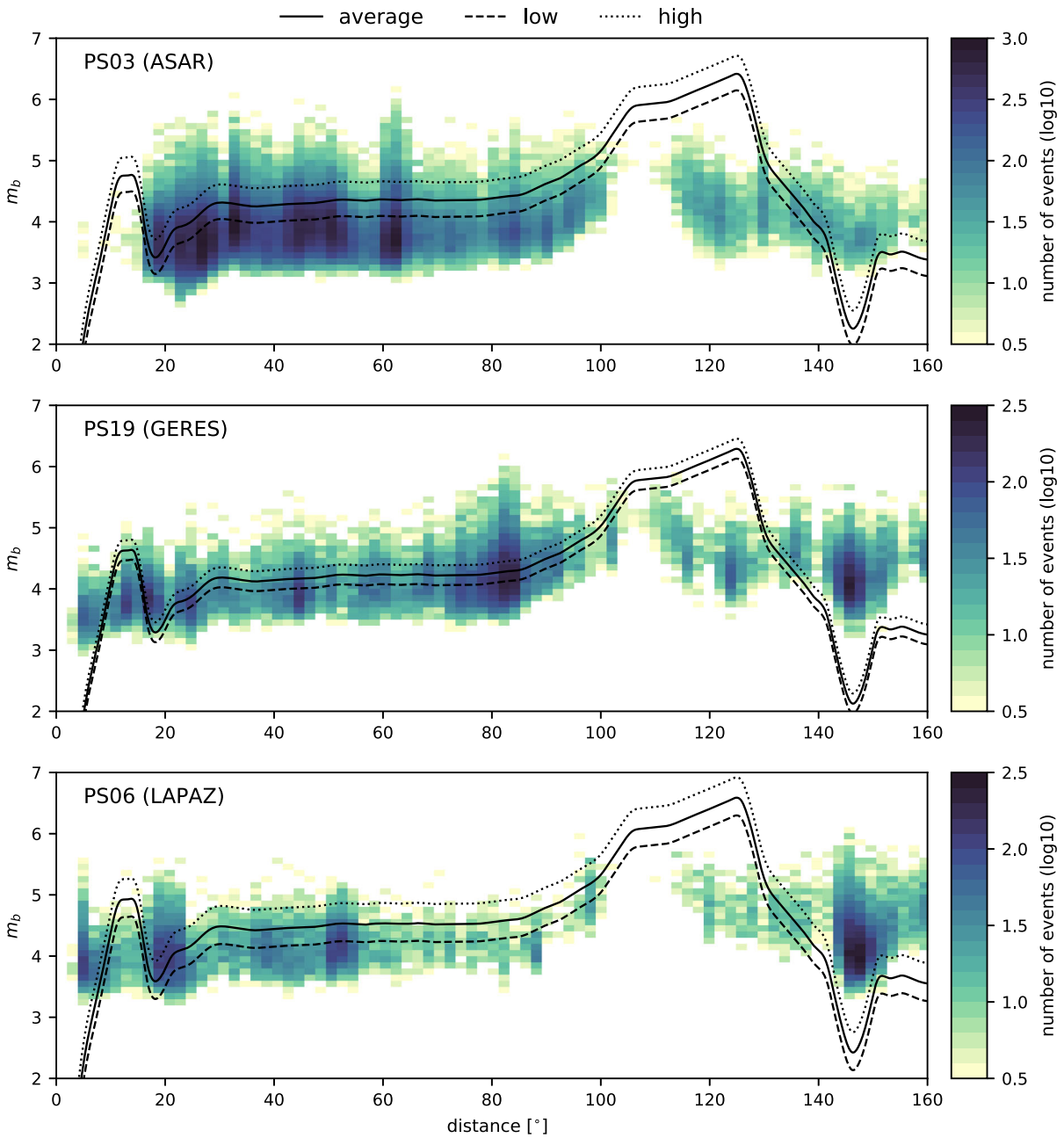

Figure 11
Comparison of theoretical and observed event magnitudes at three PS stations (PS03, PS19, PS06). Figure illustrates a comparison of distance dependent minimum observable magnitudes at the PS stations estimated using the method described in Sect. 3 to event magnitudes obtained from the REB. Lines depict the average (solid), low (dashed) and high (dotted) noise model at the PS stations. Bright background colors represent a low number of detected events, dark background colors indicate a high number of events in the REB

conservative estimation of the detection capability and even lower values might be reached in reality.

Acknowledgements

The authors of this study express their gratitude to the editors Pierrick Mialle and Martin Kalinowski for their commitment and work on the topical issue "Nuclear Explosion Monitoring and Verification: Scientific and Technological Advances". We further want to thank Tormod Kværna and an anonymous reviewer for their comments and suggestions on the manuscript. Colormaps are taken from the python package cmocean. Content presented in this study was previously published as book chapter 3 in Pilger et al. (2017): Monitoring Compliance with the Comprehensive Nuclear-Test-Ban Treaty (CTBT). Geol. Jb. B 105, 325 pages, ISBN 978-3-510-96858-9, http://www.schweizerbart.com/9783510968589.

Funding

Open Access funding enabled and organized by Projekt DEAL.

References

Bormann, P., Klinge, K., & Wendt, S. (2009). *New Manual of Seismological Observatory Practice (NMSOP), chap data analysis and seismogram interpretation* (pp. 1–102). Potsdam: Deutsches GeoForschungsZentrum GFZ.

Brown, D., Ceranna, L., Prior, M., Mialle, P., & Le Bras, R. J. (2014). The IDC seismic, hydroacoustic and infrasound global low and high noise models. *Pure and Applied Geophysics,171*(3), 361–375. https://doi.org/10.1007/s00024-012-0573-6.

Cesca, S., Heimann, S., Kriegerowski, M., Saul, J., & Dahm, T. (2017). Moment tensor inversion for nuclear explosions: What can we learn from the 6 January and 9 September 2016 nuclear tests, North Korea? *Seismological Research Letters,88*(2A), 300–310. https://doi.org/10.1785/0220160139.

Coyne, J., Bobrov, D., Bormann, P., Duran, E., Grenard, P., Haralabus, G., et al. (2012). *New Manual of Seismological Observatory Practice (NMSOP), chap CTBTO: Goals, networks, data analysis and data availability* (pp. 1–41). Potsdam: Deutsches GeoForschungsZentrum GFZ.

CTBTO. (2020). Preparatory Commission for the Comprehensive Nuclear-Test-Ban Treaty Organization. https://www.ctbto.org/.

Dziewonski, A. M., & Anderson, D. L. (1981). Preliminary reference Earth model. *Physics of the Earth and Planetary Interiors,25*(4), 297–356. https://doi.org/10.1016/0031-9201(81)90046-7.

Ekström, G., Nettles, M., & Dziewonski, A. (2012). The global CMT project 2004–2010: Centroid-moment tensors for 13,017 earthquakes. *Physics of the Earth and Planetary Interiors,200–201*, 1–9. https://doi.org/10.1016/j.pepi.2012.04.002.

Fuchs, K., & Müller, G. (1971). Computation of synthetic seismograms with the reflectivity method and comparison with observations. *Geophysical Journal of the Royal Astronomical Society,23*(4), 417–433. https://doi.org/10.1111/j.1365-246X.1971.tb01834.x.

Gaebler, P., Ceranna, L., Nooshiri, N., Barth, A., Cesca, S., & Frei, M., et al. (2019). A multi-technology analysis of the 2017 North Korean nuclear test. *Solid Earth*, *10*(1), 59–78. https://doi.org/10.5194/se-10-59-2019. https://www.solid-earth.net/10/59/2019/.

Gutenberg, B., & Richter, C. (1954). *Seismicity of the earth and associated phenomena* (2nd ed.). Princeton: Princeton University Press.

Gutenberg, B., & Richter, C. (1956). Magnitude and energy of earthquakes. *Annals of Geophysics,9*(1), 1–15.

Han, L., Wu, Z., Jiang, C., & Liu, J. (2017). Properties of three seismic events in September 2017 in the northern Korean Peninsula from moment tensor inversion. *Science Bulletin,62*(23), 1569–1571. https://doi.org/10.1016/j.scib.2017.11.007.

Harjes, H. P. (1984). Global seismic network assessment for teleseismic detection of underground nuclear explosions. Tech. rep.

Hartse, H. E., Taylor, S. R., Phillips, W. S., & Randall, G. E. (1997). A preliminary study of regional seismic discrimination in

central Asia with emphasis on western China. *Bulletin of the Seismological Society of America,87*(3), 551–568.

Haskell, N. A. (1953). The dispersion of surface waves on multilayered media*. *Bulletin of the Seismological Society of America,43*(1), 17–34.

ISC. (2020). IASPEI standard phase list. http://www.isc.ac.uk/standards/phases/

Kebeasy, R. M., Hussein, A. I., & Dahy, S. A. (1998). Discrimination between natural earthquakes and nuclear explosions using the Aswan Seismic Network. *Annali Di Geofisica,41*(2), 127–140.

Kennett, B. (1983). *Seismic wave propagation in stratified media*. Cambridge: Cambridge University Press.

Kennett, B. L. N., Engdahl, E. R., & Buland, R. (1995). Constraints on seismic velocities in the Earth from travel times. *Geophysical Journal International,122*(1), 108–124. https://doi.org/10.1007/s00024-012-0573-60.

Kværna, T., & Ringdal, F. (1999). Seismic threshold monitoring for continuous assessment of global detection capability. *Bulletin of the Seismological Society of America,89*(4), 946–959.

Kværna, T., & Ringdal, F. (2013). Detection capability of the seismic network of the international monitoring system for the Comprehensive Nuclear-Test-Ban Treaty. *Bulletin of the Seismological Society of America,103*(2A), 759–772. https://doi.org/10.1007/s00024-012-0573-61.

Liu, J., Li, L., Zahradník, J., Sokos, E., Liu, C., & Tian, X. (2018). North Korea's 2017 test and its nontectonic aftershock. *Geophysical Research Letters,45*(7), 3017–3025. https://doi.org/10.1007/s00024-012-0573-62.

Müller, G. (1985). The reflectivity method: A tutorial. *Journal of Geophysics,58*(1–3), 153–174.

Murphy, J. R. (1981). *Identification of seismic sources–Earthquake or underground explosion, chap P wave coupling of underground explosions in various geologic media* (pp. 201–205). Berlin: Springer.

Murphy, J. R., & Barker, B. W. (2003). Revised distance and depth corrections for use in the estimation of short-period P-wave magnitudes. *Bulletin of the Seismological Society of America,93*(4), 1746–1764. https://doi.org/10.1007/s00024-012-0573-63.

National Research Council. (2012). *The comprehensive nuclear test ban treaty: Technical issues for the United States*. Washington, DC: The National Academies Press.

Pilger, C., Ceranna, L., & Bönnemann, C. (2017). *Monitoring compliance with the Comprehensive Nuclear-Test-Ban Treaty (CTBT) contributions by the German National Data Center*. Stuttgart: Schweizerbart Science Publishers.

Qamar, A. (1973). Revised velocities in the Earth's core. *Bulletin of the Seismological Society of America,63*(3), 1073–1105.

Rezapour, M. (2003). Empirical global depth-distance correction terms for mb determination based on seismic moment. *Bulletin of the Seismological Society of America,93*(1), 172–189. https://doi.org/10.1007/s00024-012-0573-64.

Richards, P. G., & Kim, W. Y. (2007). Seismic signature. *Nature Physics,3*, 4–6. https://doi.org/10.1007/s00024-012-0573-65.

Ringdal, F. (1986). Study of magnitudes, seismicity, and earthquake detectability using a global network. *Bulletin of the Seismological Society of America,76*(6), 1641–1659.

Ringdal, F., & Kværna, T. (1989). A multi-channel processing approach to real time network detection, phase association, and threshold monitoring. *Bulletin of the Seismological Society of America,79*(6), 1927–1940.

Ringdal, F., & Kværna, T. (1992). Continuous seismic threshold monitoring. *Geophysical Journal International,111*(3), 505–514. https://doi.org/10.1007/s00024-012-0573-66.

Ringdal, F., Marshall, P. D., & Alewine, R. W. (1992). Seismic yield determination of Soviet underground nuclear explosions at the Shagan River test site. *Geophysical Journal International,109*(1), 65–77. https://doi.org/10.1007/s00024-012-0573-67.

Rost, S., & Thomas, C. (2002). Array seismology: Methods and applications. *Reviews of Geophysics,40*(3), 2-1–2-27. https://doi.org/10.1007/s00024-012-0573-68.

Thomson, W. T. (1950). Transmission of elastic waves through a stratified solid medium. *Journal of Applied Physics,21*(2), 89–93. https://doi.org/10.1007/s00024-012-0573-69.

Veith, K. F., & Clawson, G. E. (1972). Magnitude from short-period P-wave data. *Bulletin of the Seismological Society of America, 62*(2), 435–452.

(Received December 7, 2019, revised July 24, 2020, accepted October 10, 2020, Published online January 25, 2021)